Journal of Thermal Science Vol.32, No.4 (2023) 1614−1625

**https://doi.org/10.1007/s11630-023-1843-6** **Article ID: 1003-2169(2023)04-1614-12**

# Investigation on a Supercritical Water Gasification System with $CO_2$ as Transporting Medium

**WANG Weizuo, LU Bingru, SHI Jinwen, ZHAO Qiuyang, JIN Hui***

State Key Laboratory of Multiphase Flow in Power Engineering (SKLMF), Xi'an Jiaotong University, Xi'an 710049, China



**Abstract:** As a benign energy vector, hydrogen has been discussed for a long time. Supercritical water gasification was one of good ways to produce hydrogen. However, supercritical water gasification system with $H_2O$ transporting was energy consuming in the process of heating due to the high specific heat of $H_2O$. A new supercritical water gasification system was established in this paper with supercritical $CO_2$ as medium instead. Phenolic plastics were used as the sample transported by $CO_2$. Production yields, energy flow and exergy flow of the system were collected and the influence of temperature, pressure, gasification concentration and transporting concentration was investigated. Mass flow of $H_2O$ input into the reactor was 1000 kg/h. The typical condition was as follow: temperature 923.15 K, pressure 23 MPa, and the mass ratio of water, sample and transporting medium was 100 : 9 : 9. Yield of $H_2$, $CH_4$, CO and $CO_2$ at this condition was 8.1 kg/h, 39.6 kg/h, 6.6 kg/h and 137.5 kg/h, respectively. Similar system with $H_2O$ transporting was used to compare with the supercritical $CO_2$ transporting system and proved that system with $CO_2$ transporting could reduce the loss of both energy and exergy while the reduce of each gas production yield was less than 0.1 mol/mol.

**Keywords: phenolic plastics, supercritical water gasification, $CO_2$-transporting system, energy and exergy flow**

## 1. Introduction

With the increasing demand of energy, traditional carbon fuels will be more scarce and expensive, and there are also environmental issues such as global warming and incidental pollution [1]. In the current research on green and renewable energy, hydrogen energy is widely considered as one of the ideal energy sources due to its high energy content per unit weight and the clean combustion products [2].

There are many methods for clean hydrogen production, among which supercritical water gasification has a high hydrogen production potential [3]. The principle is that organic matter reacted with supercritical water to produce hydrogen-based combustible gas. The physical properties of water change dramatically above critical point (647.15 K, 22.1 MPa). Supercritical water has the characteristics of high diffusivity and high solubility. Taking advantage of these properties, supercritical water can gasify organic matter such as coal, biomass, and plastics [4–7]. In the gasification reaction, water acts as both reactant and catalyst in the supercritical phase [8], and this reaction also has the advantages of short reaction time, complete reaction, and cleanness [9].

At present, many researchers have conducted thermodynamic analysis on supercritical water

Article type: Invited article
Received: Feb 8, 2023
AE: LI Yinshi
Corresponding author: JIN Hui E-mail: jinhui@mail.xjtu.edu.cn

gasification technology, and thermodynamic analysis can provide a basis for system optimization in terms of efficiency [10]. Our group [11] studied the thermodynamic properties of coal supercritical water gasification under different concentrations, pressures and temperatures. The results showed that higher concentrations, pressures and temperatures led to better thermodynamic properties. Aziz [12] proposed a new hydrogen production and power generation integrated system based on supercritical water gasification. Microalgae were selected as samples for process simulation, and the effects of steam flow, gasification pressure and turbine inlet temperature on the total energy efficiency of the system were studied. The results showed that the proposed integrated process harvested energy from microalgae with an overall energy efficiency of more than 40%, and the heat involved in the whole process was effectively recovered. Rahbari et al. [13] used Aspen Plus to control the algae biomass heated by solar energy. Energy analysis and exergy analysis were carried out for high-quality supercritical water gasification, and the results showed that the exergy efficiency of the system dropped sharply when the concentration of algae decreased. It was explained that more energy was required to heat up water and higher exergy lost at lower concentration.

In conventional continuous gasification reactors, water was used to transport feedstock [14–16]. However, water has large specific heat capacity and low heating rate, which lead to high energy-consuming transaction and by side reaction products. Therefore, we set our sights on $CO_2$. However, there was still a lack of relevant reports on $CO_2$ transport in SCWG systems. Unlike water, the critical point of $CO_2$ is 304.45 K and 7.38 MPa. $CO_2$ with a lower critical point can easily cross the large specific heat region and has little impact on the heating process. In previous studies, supercritical $CO_2$ had the ability to carry feedstock [17–20]. The system with $CO_2$ as the transporting medium was expected to reduce heat input into the system and then save the energy consumption.

On the other hand, this paper took phenolic plastics as a sample and transported it with $CO_2$. There was no doubt that the widespread use of plastics not only facilitated human society, but also caused environmental pollution that was difficult to clean up and recycle [21]. The use of $CO_2$ to transport phenolic plastics also provided new ideas and means for the recycling of thermosetting plastics.

Based on these goals, a supercritical water gasification system using $CO_2$ as transporting medium was established in this paper. The effects of temperature, pressure, feedstock concentration and other factors on the system were investigated. The reaction results were valued by the amount of gas produced, the mole fraction of gas produced, the total yield and the hydrogen conversion rate. Furthermore, energy and exergy flows were aggregated and compared with the $H_2O$ transport system.

## 2. Materials and Methods

### 2.1 Materials

Thermosetting plastics were thought as one of the most difficult substances for recycling due to its highly cross-linked structure [22]. As a kind of typical thermosetting plastics, phenolic plastics were widely used and many types of modifiers were used to modify its molecular structure [23]. Phenolic plastics adhesive were one of the main adhesives and used in many applications, such as laminate, automobile, aerospace and many other fields [24]. Many researchers had tried to recycle the plastics for more than 20 years [25–28].

The chemical structures of phenolic plastics were shown in Fig. 1. Molecular formula of the structure A was $C_{(7n+13)}H_{(6n+12)}O_{(n+2)}$ and the molecular formula of the structure B was $C_{(7m+8n)}H_{(6m+8n)}O_{(3m+2n)}$. The mass fraction of C, H and O was in the range of 78.45 wt% to 79.08 wt%, 5.77 wt% to 5.71 wt% and 15.38 wt% to 15.22 wt% when $n$ changed from 4 to 12 in acidic preparation. The median value was used as the mass fraction in this paper.

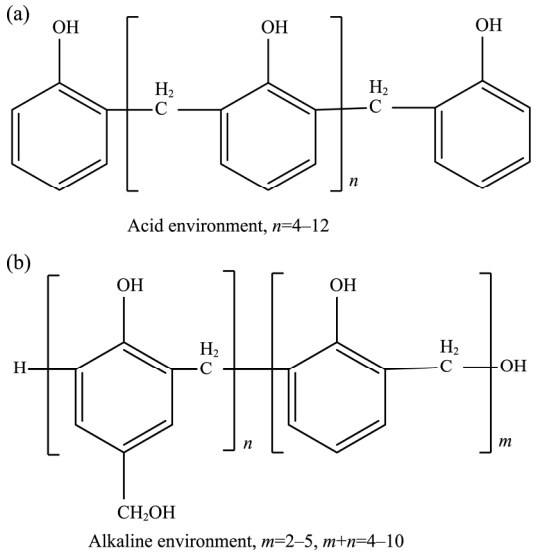


**Fig. 1** Chemical structure of phenolic plastics (a) Acidic preparation; (b) Alkaline preparation

### 2.2 Structure of system

Flowchart of the system was shown in Fig. 2, in which each flow was made up with one or more of these substances: $H_2$, $CH_4$, CO, $CO_2$, $H_2O$ and plastics. According to the law of conservation of mass, the total mass flow was the numerical sum of the mass flow of each substance. As a result, matrix $\boldsymbol{M}_x$, $\boldsymbol{N}_x$ was used to

record the mass flow (kg/h) and mole flow (kmol/h) of each substance in flow $x$, respectively. Mass enthalpy (kJ/kg) and mass entropy (kJ/(kg·K)) in each flow was recorded in matrix $\boldsymbol{H}_x$ and $\boldsymbol{S}_x$, respectively. $\boldsymbol{H}_0$ and $\boldsymbol{S}_0$ meant the mass enthalpy (kJ/kg) and mass entropy (kJ/(kg·K)) at the condition of normal temperature and pressure (298.15 K, 0.1 MPa). The lower heating value and standard chemical exergy were recorded in matrix **LHV** and $\boldsymbol{EX}_q$. $\boldsymbol{EX}_q$ was calculated by Kameyama-Yoshida environmental model with temperature correction.

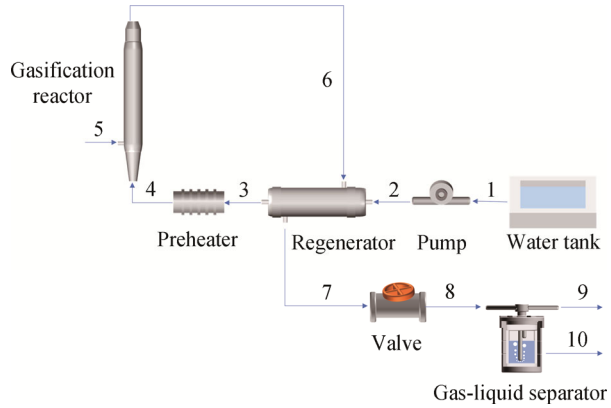


**Fig. 2** Flowchart of the system with $CO_2$ transporting

$$\boldsymbol{M}_x = \left[ m_{\mathrm{H_2}} \quad m_{\mathrm{CH_4}} \quad m_{\mathrm{CO}} \quad m_{\mathrm{CO_2}} \quad m_{\mathrm{H_2O}} \quad m_{\mathrm{Plastics}} \right]^{\mathrm{T}} \tag{1}$$

$$\begin{aligned} \boldsymbol{N}_x &= \left[ n_{\mathrm{H_2}} \quad n_{\mathrm{CH_4}} \quad n_{\mathrm{CO}} \quad n_{\mathrm{CO_2}} \quad n_{\mathrm{H_2O}} \quad n_{\mathrm{Plastics}} \right]^{\mathrm{T}} \\ &= \left[ \frac{m_{\mathrm{H_2}}}{2} \quad \frac{m_{\mathrm{CH_4}}}{16} \quad \frac{m_{\mathrm{CO}}}{28} \quad \frac{m_{\mathrm{CO_2}}}{44} \quad \frac{m_{\mathrm{H_2O}}}{18} \quad \frac{m_{\mathrm{Plastics}}}{M_{\mathrm{Plastics}}} \right]^{\mathrm{T}} \end{aligned} \tag{2}$$

$$\boldsymbol{H}_x = \left[ h_{\mathrm{H_2}} \quad h_{\mathrm{CH_4}} \quad h_{\mathrm{CO}} \quad h_{\mathrm{CO_2}} \quad h_{\mathrm{H_2O}} \quad h_{\mathrm{Plastics}} \right] \tag{3}$$

$$\boldsymbol{S}_x = \left[ s_{\mathrm{H_2}} \quad s_{\mathrm{CH_4}} \quad s_{\mathrm{CO}} \quad s_{\mathrm{CO_2}} \quad s_{\mathrm{H_2O}} \quad s_{\mathrm{Plastics}} \right] \tag{4}$$

$$\mathbf{LHV} = \left[ \mathrm{LHV}_{\mathrm{H_2}} \quad \mathrm{LHV}_{\mathrm{CH_4}} \quad \mathrm{LHV}_{\mathrm{CO}} \quad 0 \quad 0 \quad \mathrm{LHV}_{\mathrm{Plastics}} \right] \tag{5}$$

$$\beta = \frac{1.0414 + 0.177 \times \dfrac{[\mathrm{H}]}{[\mathrm{C}]} - 0.3328 \times \dfrac{[\mathrm{O}]}{[\mathrm{C}]} \times \left( 1 + 0.0537 \times \dfrac{[\mathrm{H}]}{[\mathrm{C}]} \right)}{1 - 0.4021 \times \dfrac{[\mathrm{O}]}{[\mathrm{C}]}} \tag{6}$$

$$\boldsymbol{EX}_{\mathrm{q}} = \left[ EX_{\mathrm{q_{H_2}}} \quad EX_{\mathrm{q_{CH_4}}} \quad EX_{\mathrm{q_{CO}}} \quad EX_{\mathrm{q_{H_2O}}} \quad 0 \quad \beta \times \mathrm{LHV}_{\mathrm{Plastics}} \right] \tag{7}$$

Moreover, the energy $En_x$ (kJ) and exergy $Ex_x$ (kJ) of flow $x$ could be calculated by Eqs. (8) and (9).

$$\begin{aligned} En_x &= En_{\mathrm{ph}x} + En_{\mathrm{ch}x} \\ &= \left\| \left( \boldsymbol{H}_x - \boldsymbol{H}_0 \right) \times \boldsymbol{M}_x \right\| + \left\| \mathbf{LHV} \times \boldsymbol{M}_x \right\| \end{aligned} \tag{8}$$

$$\begin{aligned} Ex_x &= Ex_{\mathrm{ph}x} + Ex_{\mathrm{ch}x} \\ &= \left\| \left[ \left( \boldsymbol{H}_x - \boldsymbol{H}_0 \right) - T_0 \left( \boldsymbol{S}_x - \boldsymbol{S}_0 \right) \right] \times \boldsymbol{M}_x \right\| \\ &\quad + \left\| \boldsymbol{EX}_{\mathrm{q}} \times \boldsymbol{M}_x \right\| + \Delta E_{\mathrm{diffusion}} \end{aligned} \tag{9}$$

Shown in Fig. 2, $H_2O$ from the tank (flow 1) was pressurized by the pump (flow 2) and then be heated in the regenerator (flow 3) and preheater (flow 4). The efficiency of the pump was 90%. As a result, $H_2O$ output from the preheater (flow 4) reached the set reaction conditions and it was at supercritical phase. The regenerator was a heat exchanger whose efficiency was set to 90% and the temperature difference between the output of cold flow and the input of hot flow was set to 473.15 K. Heat efficiency of preheater was 90%. Energy and exergy flow of these models could be calculated by Eqs. (10) to (15).

$$W_{\mathrm{pump}} = \frac{En_2 - En_1}{\eta_{\mathrm{pump}}} \tag{10}$$

$$\Delta EX_{\mathrm{pump}} = \frac{EX_2 - EX_1}{\eta_{\mathrm{pump}}} \tag{11}$$

$$En_7 = En_6 - \frac{En_3 - En_2}{\eta_{\mathrm{regenerator}}} \tag{12}$$

$$Q_{\mathrm{preheater}} = \frac{En_4 - En_3}{\eta_{\mathrm{preheater}}} \tag{13}$$

$$\Delta EX_{\mathrm{preheater}} = Q_{\mathrm{preheater}} \times \left( 1 - \frac{T_0}{(T + T_0)/2} \right) \tag{14}$$

$$\eta_{\mathrm{Xpreheater}} = 1 - \frac{T_0}{(T_3 + T_4)/2} \tag{15}$$

where $\eta_{\mathrm{preheater}}$ and $\eta_{\mathrm{Xpreheater}}$ represented the energy and exergy efficiency of the preheater in this system. The input flows of gasification reactor were the flow of $H_2O$ in supercritical phase (flow 4) and the flow of the mixture of carbon dioxide and plastics (flow 5). Gasification reaction could be divided into four reactions, steam reforming reaction (16), water-gas shift reaction (17) and methanation reactions (18) and (19) [29]. The Gibbs free energy in this system would tend to be minimum in gasification reaction. Afterwards, the products flow of the reaction could be calculated. Heat

efficiency of reactor was set to 90% and heat absorption of the reactor equaled the difference between the energy of input flow and output flow, as shown in formula (20) and (21).

$$\text{Plastics} + H_2O \rightarrow CO + CO_2 + H_2 \quad (16)$$

$$CO + H_2O \rightarrow CO_2 + H_2 \quad (17)$$

$$CO + 3H_2 \rightarrow CH_4 + H_2O \quad (18)$$

$$CO_2 + 4H_2 \rightarrow CH_4 + 2H_2O \quad (19)$$

$$Q_{\text{reactor}} = \frac{En_6 - En_5 - En_4}{\eta_{\text{reactor}}} \quad (20)$$

$$\Delta EX_{\text{reactor}} = Q_{\text{reactor}}\left[1-(T_0/T)\right] \quad (21)$$

Flow out of gasification reactor (flow 6) contained a large amount of supercritical $H_2O$, some $CO_2$ and fuel gas products, such as $H_2$, CO and $CH_4$. It would transfer the heat to flow 2 in the regenerator. Pressure of flow 7 would be released to 4 MPa in the pressure reducing valve. $H_2O$ was liquefied in regenerator and finally separated in the separator. Liquid phase (flow 10) flew out of the separator flowed into the water tank for recycle. Gas phase flow (flow 9) contained $CO_2$ and the fuel gas products.

### 2.3 Measurement parameters

Temperature, pressure, the mass ratio of sample to $H_2O$ (Sample/ $H_2O$) and that of sample to $CO_2$ (Sample/ CO2) were changed and their influence on the gasification was investigated. Yield, mass fraction of the products, energy flows and exergy flows of each model in the system were all calculated. Hydrogen conversion rate (HE) and carbon conversion rate (CE) of gasification were also calculated. The mass flow in flow 6 of $H_2$, $CH_4$ and CO equaled the yield of the corresponding products. And the yield of $CO_2$ was the difference of its mass flow in the output flow (flow 6) and the input flow (flow 5).

$$HE = \frac{m_{H_2} + \frac{1}{4}m_{CH_4}}{m_{\text{sample}} \times \omega_H} \times 100\% \quad (22)$$

*HE* represented the conversion rate of hydrogen; *m* represented the mass flow of each substance in the flow; $H_2$ and $CH_4$ was the products of gasification in flow 6 while sample was the ingredient in flow 5; $\omega_H$ was the mass fraction of element H in the sample.

## 3. Results and Discussion

Mass flow of $H_2O$ input into the reactor was set to 1000 kg/h and the typical condition was as follow: temperature 923.15 K, pressure 23 MPa, and the mass ratio of $H_2O$, sample and transporting medium was 100:9:9. Temperature changed from 873.15 K to 1073.15 K and pressure changed from 23 MPa to 29 MPa, independently. Mass flow of sample and carbon dioxide changed at 923.15 K and 23 MPa. In this way, influence of the mass ratio of water, sample and carbon dioxide could be investigated.

### 3.1 Effect on the production yields

It was shown in Fig. 3(a) that yields of $H_2$, CO and $CO_2$ increased with temperature while the yield of $CH_4$ decreased. At low temperature, the products were mainly $H_2$, $CH_4$ and $CO_2$. As temperature increased, mole fraction of $H_2$ and CO increased while those of $CH_4$ and $CO_2$ decreased, as shown in Fig. 3(b). Mole fraction of $H_2$ increased to almost 0.60 mol/mol at 1,073.15 K. Total yield increased with temperature, as shown in Fig. 3(e). HE showed the same trend as the yield shown in Fig. 3(f).

Fig. 3(c) and Fig. 3(d) showed that the influence of pressure was not as obvious as that of temperature. Yields of $H_2$, CO and $CO_2$ decreased with pressure. Mole fractions of $CH_4$, CO and $CO_2$ increased with pressure while mole fraction of $H_2$ decreased. The total yield also decreased with pressure, so did the HE.

Previous study on corn stover attributed the effect of temperature to the heat absorption and release of the reaction [30]. The steam reforming reaction (16) and water-gas reaction (17) were endothermic reaction which could be promoted by high temperature. Meanwhile, methanation reactions (18) and (19) were exothermic reaction inhibited by high temperature. CO was the product in the reverse reaction of methanation reactions (18) and (19). As a result, yield of $H_2$, CO and $CO_2$ increased with temperature and yield of $CH_4$ decreased at the same time. Besides, the promotion of steam reforming reaction (16) water-gas reaction (17) participated in the reaction. Reactant of gasification reaction was the feedstock and $H_2O$ and the products were the fuel gas. Total yield equaled the mass of reactant according to the energy conservation equation. Total yield increased with the increase of $H_2O$ in reactant. HE was the quotient of hydrogen in products and sample. Therefore, both total yield and HE increased with temperature.

According to the Le Chatelier's principle, the increase of pressure could inhibit the steam reforming reaction (16) and promote the methanation reactions (18) and (19) [6]. The influence of pressure was not obviously contrary to that of temperature.

The solid phase volume fraction of the system transported by supercritical $CO_2$ along horizontal direction was in the range of 10 vol% to 20 vol% [17]. The mass fraction of sample in flow 8, defined as the transporting concentration, was calculated in the range of 16.7 wt% to 54.5 wt%. Fig. 4(a) showed that the yield of $H_2$ and $CO_2$ increased with the increase of transporting concentration and that of $CH_4$ and CO decreased. Mole fractions of each gas changed no more than 0.05 mol/mol when changing the transporting concentration. The

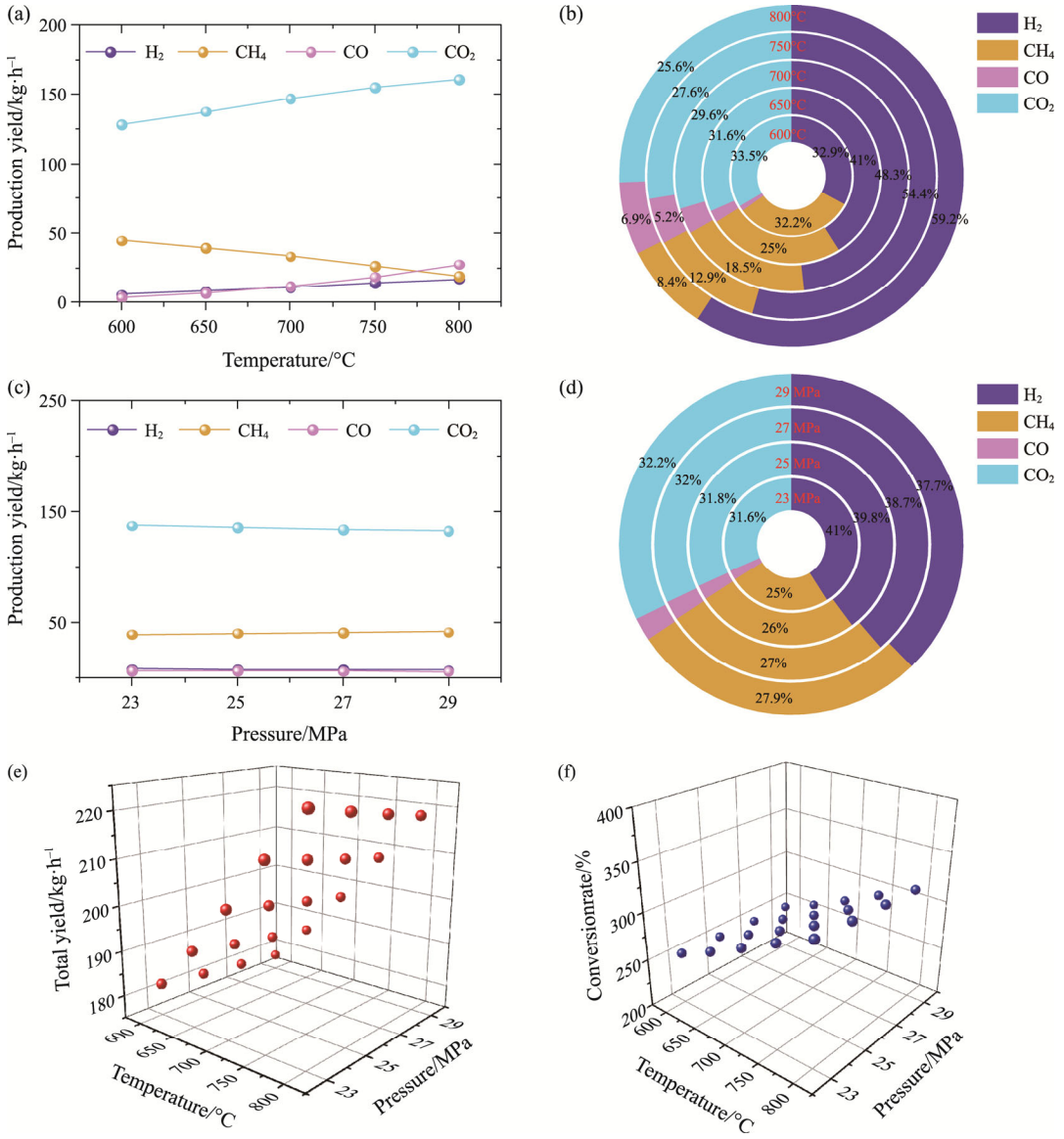


**Fig. 3** Influence of temperature on (a) each gas production yield and (b) mole fraction of each gas production; Influence of pressure on (c) each gas production yield and (d) mole fraction of each gas production; (e) Total production yield and (f) Hydrogen conversion rate at each temperature and pressure

gasification concentration was positively correlated to the quotient of sample and $H_2O$ input into gasification reactor. Yield of each product increased almost linearly with gasification concentration, as shown in Fig. 4(c). Fig. 4(d) showed that mole fraction of $CO_2$ in products was stable in the range of 0.29 mol/mol to 0.32 mol/mol. At the same time, mole fraction of $CH_4$ increased sharply and that of $H_2$ decreased from 0.62 mol/mol to 0.36 mol/mol. Increase of the transporting concentration led to the increase of the total yield, as shown in Fig. 4(e). This trend was slow at high transporting concentration. Total yield increased with gasification concentration almost linearly. Meanwhile, HE increased with transporting concentration but decreased with gasification concentration.

The mass flow of input $CO_2$ decreased with transporting concentration. According to the Le Chatelier's principle, lower mass flow of $CO_2$ could promote the steam reforming reaction (18) and water-gas reaction (19) and inhibit one of methanation reactions (21) at the same time. Therefore, the yields of $H_2$, CO and $CO_2$ increased and that of $CH_4$ decreased with transporting concentration. Gas yield increased with gasification concentration but the mass ratio of gas production and sample decreased. The results were consistent with the previous research [29]. High gasification concentration meant more sample gasified. And the gas yield increased. However, the experimental results also showed the gasification effects turned to worse at high gasification concentration [6]. The mass

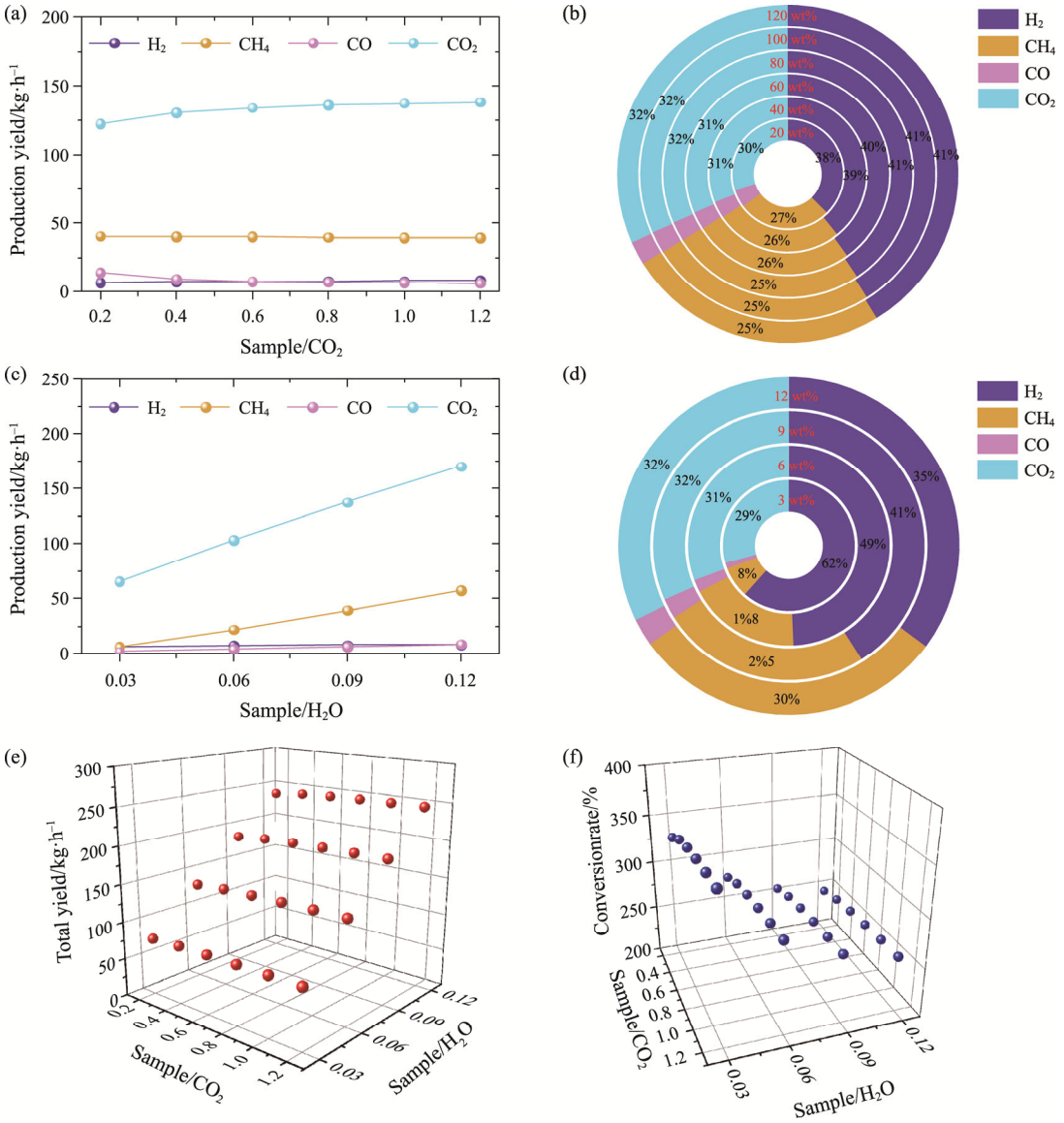


**Fig. 4** Influence of transporting concentration on (a) each gas production yield and (b) mole fraction of each gas production; Influence of gasification concentration on (c) each gas production yield and (d) mole fraction of each gas production; (e) Total production yield and (f) Hydrogen conversion rate at each transporting and gasification concentration

ratio of sample to $H_2O$ was low at high gasification concentration [9, 31]. Steam reforming reaction (16) and water-gas reaction (17) would be inhibited by the ratio. As a result, the gasification production yield and hydrogen conversion rate turned to less.

### 3.2 Effect on the electricity consumption of gasification reactor

It could be seen in Fig. 5(a) that the electricity consumption of the reactor increased with temperature and decreased with pressure. The electricity consumption could be divided into three parts. The first one was electricity to heat the transporting medium in flow 5 which increased almost linearly with temperature and little affected by pressure, as shown in Fig. 5(b). The second part was the heat absorption of gasification reaction. It was proved that gasification was the endothermic reaction at low gasification concentration [32]. Fig. 5(c) showed that the reaction heat absorption increased with temperature and decreased with pressure. The last one was the heat loss, containing 10% of whole electricity consumption at 90% efficiency of reactor.

Electricity consumption of the first part was the difference between enthalpy value of transporting medium and sample at reaction condition and that of flow 5. It would cost much electricity to heat the fluid and the specific heat capacity was stable at high temperature. As a result, influence of temperature was obvious and almost linear. Electricity consumption of the second part was related to the reactions. It was concerned

that high temperature could promote the endothermic steam reforming reaction (16) and water-gas reaction (17) and inhibit the exothermic methanation reactions (18) and (19). With the increase of temperature, yields of $CH_4$ decreased and yields of other products increased. More energy absorbed in the endothermic reactions and less heat released from the exothermic reactions. Steam reforming reaction (16) was inhibited while methanation

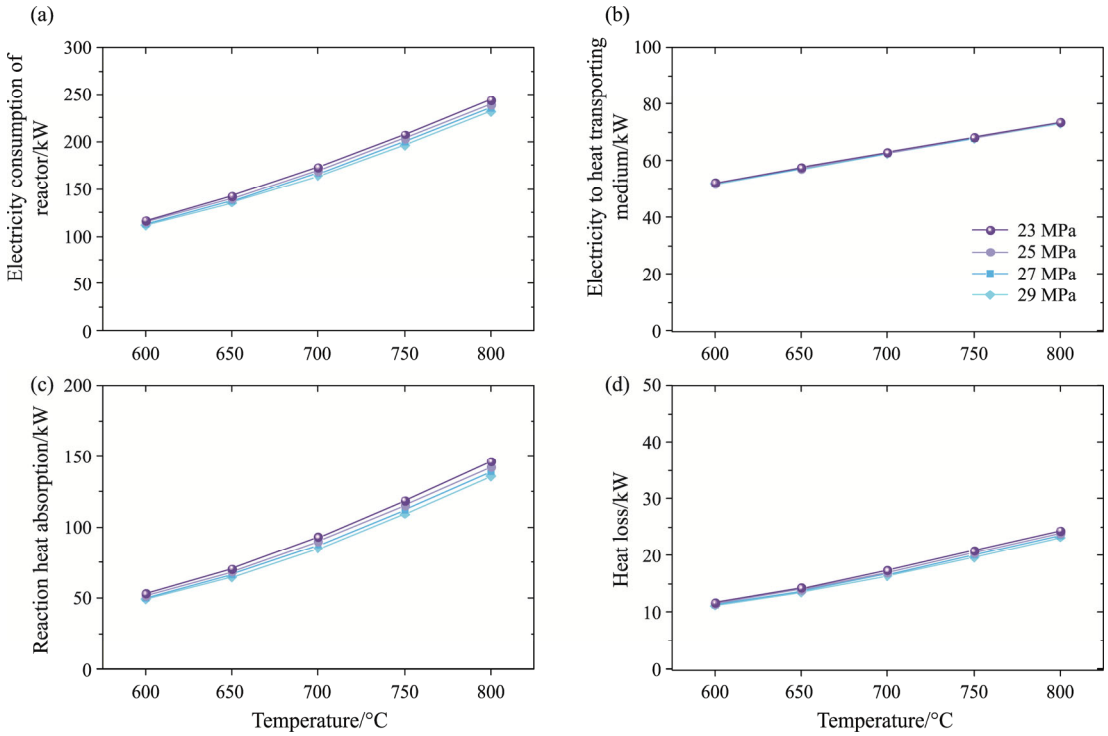


**Fig. 5** (a) Electricity consumption; (b) Electricity to heat transporting medium; (c) Reaction heat absorption; (d) Heat loss at each temperature and pressure

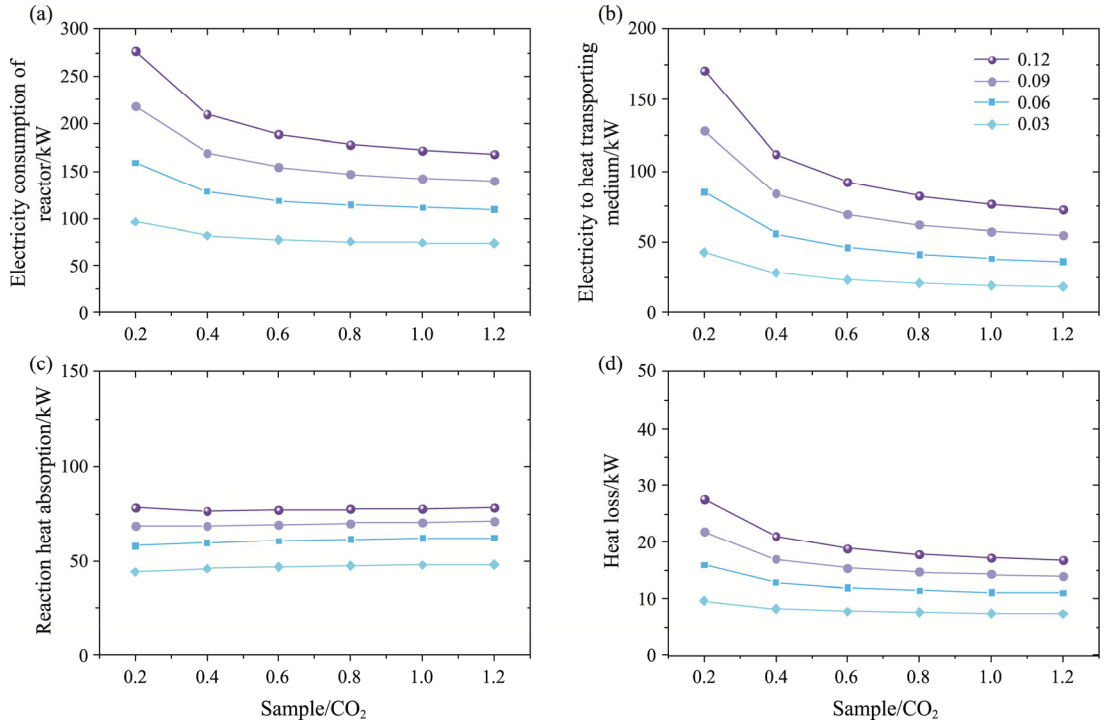


**Fig. 6** (a) Electricity consumption; (b) Electricity to heat transporting medium; (c) Reaction heat absorption; (d) Heat loss at each transporting and gasification concentration

reactions were promoted with pressure according to the Le Chatelier's principle. Therefore, the influence of pressure showed the trend opposite to the influence of temperature. Electricity consumption of the third part equaled 10% of total electricity consumption of the reactor and had the same trend of total electricity consumption.

Fig. 6(a) showed that heat absorption decreased with transporting concentration. The increase of gasification concentration promoted the heat absorption and became stable at high transporting concentration. Fig. 6(b) and Fig. 6(d) showed that energy to heat transporting medium and the heat loss had the same trend with the total electricity consumption of reactor. Heat absorption of gasification reaction increased with gasification concentration as shown in Fig. 6(c). The influence of transporting concentration was no more than 5%.

Energy to heat transporting medium increased when the mass flow of sample and $CO_2$ increased. The increase of gasification concentration led to the increase of mass flow of plastics sample. At same gasification concentration, high transporting concentration meant low mass flow of $CO_2$. The result was that the increase of gasification concentration and decrease of transporting concentration would increase the electricity input in the first part mentioned in former chapter. The mass flow of sample increased with gasification concentration which promoted the total gasification reaction and more energy was absorbed in the second part. The increase of $CO_2$ input into the gasification reactor influenced the reaction slightly, especially at high transporting concentration. Therefore, the heat absorption of reaction was also influenced slightly. Heat loss of the third part had the same trend with the total electricity consumption.

## 4. Compare the Transporting Medium of $CO_2$ as with $H_2O$

At the typical working condition (Temperature 923.15 K; Pressure 23 MPa; the mass ratio of $H_2O$, sample and transporting medium was 100:9:9), the transporting medium was set as $H_2O$ and $CO_2$, respectively. The gasification reactions and the systems were investigated to research the influence of different transporting mediums.

### 4.1 Comparison of the gasification reactions

Thermochemical equation was used to reflect the gasification reaction. The chemical stoichiometric coefficients of the thermochemical equation were calculated by mass flow of each content. And the endothermic quantity equaled the sum of heat absorption of three parts according to Hess's law, as shown in Fig. 7. The first part was cooling part whose heat release equaled the heat released by the reactants from the reaction condition down to normal temperature and pressure. The second part was reaction part and its endothermic quantity was the difference between the enthalpy of formation of products and reactants. The third part was heating part in which heat absorption equaled the heat absorbed by the products from normal temperature and pressure to reaction condition.

The production yields were shown in Fig. 8. The total yield of the gasification increased about 5 wt% in $H_2O$-transporting system than that in $CO_2$-transporting system. The yields of $H_2$ and $CO_2$ increased at the same time. It could be explained that the increase of $H_2O$ and decrease of $CO_2$ in flow 5 promoted steam reforming reaction (16) and water-gas shift reaction (17) and inhibited the methanation reactions (18) and (19).

Thermochemical equations of double systems were as follows:

Thermochemical equation with $H_2O$ transporting:

$$\mathrm{Plastics(s)} + 7.25\mathrm{H_2O(sc)} \xrightarrow{923.15\ \mathrm{K}\ \ 23\ \mathrm{MPa}} 5.68\mathrm{H_2(sc)} + 2.78\mathrm{CH_4(sc)} + 0.20\mathrm{CO(sc)} + 4.03\mathrm{CO_2(sc)} \quad \Delta H_1 = 322.70\ \mathrm{kJ/mol} \tag{23}$$

Thermochemical equation with $CO_2$ transporting:

$$\mathrm{Plastics(s)} + 6.79\mathrm{H_2O(sc)} \xrightarrow{923.15\ \mathrm{K}\ \ 23\ \mathrm{MPa}} 4.87\mathrm{H_2(sc)} + 2.97\mathrm{CH_4(sc)} + 0.28\mathrm{CO(sc)} + 3.75\mathrm{CO_2(sc)} \quad \Delta H_2 = 289.90\ \mathrm{kJ/mol} \tag{24}$$

The comparison of production yields and the thermochemical equations showed that the influence of different transporting mediums influenced the reaction was no more than 10%. When the transporting medium was changed from $CO_2$ to $H_2O$, the yield of $H_2$ increased from 8.11 kg/h to 9.46 kg/h; that of $CH_4$ decreased form 39.58 kg/h to 37.01 kg/h; that of CO decreased from 6.57 kg/h to 4.58 kg/h and that of $CO_2$ increased from 137.54 kg/h to 147.75 kg/h. And the heat absorptions of the gasification in double systems were 70.76 kW and 76.00 kW, respectively.

### 4.2 Comparison of the systems

Electricity input into the system with $H_2O$ transporting equaled 430.72 kW while that with $CO_2$ transporting was 344.49 kW, as shown in Fig. 9. $CO_2$-transporting system saved about 86.23 kW and this part of energy was mainly saved in gasification reactor. In the gasification reactor,

electricity consumption could be divided into three parts. Electricity to heat transporting medium was significantly saved due to the low critical point of $CO_2$. The difference of reaction heat absorption was less than 10% as mentioned in Section 4.1.

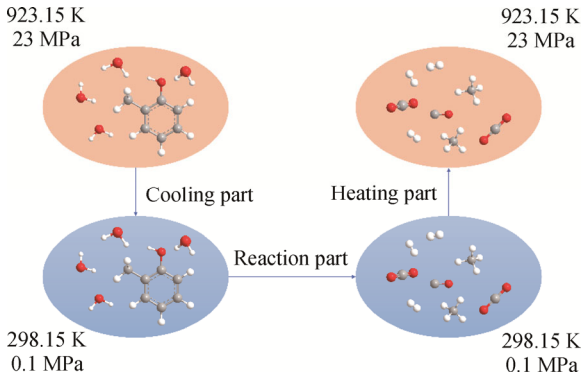


**Fig. 7** Schematic diagram of Hess's law

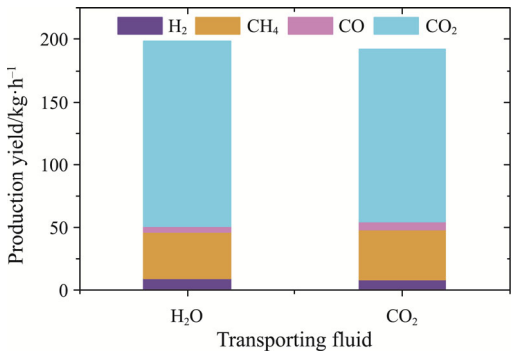


**Fig. 8** Production yield of the gasification with different transporting medium

As shown in Fig. 9, the difference of energy loss between double systems was 103.48 kW and that of exergy loss was 78.97 kW. Both energy loss and exergy loss were low in the $CO_2$-transporting system. The energy efficiency of double systems was 77.4% in $H_2O$-transporting system and 82.53% in $CO_2$-transporting system, respectively. The exergy efficiency was 68.42% and 73.11%, respectively. It proved that the system with $CO_2$ transporting had low energy and exergy loss and high energy and exergy efficiency.

The gasification reactor and preheater occupied most of electricity input of the both systems. The electricity input into these two models was used for supercritical water environment. The way to reduce the consumption was increasing the efficiency of these models. The energy loss of the systems concentrated on regenerator, valve, gasification reactor and preheater. As the model with the most energy loss, regenerator had high temperature difference due to the existence of critical

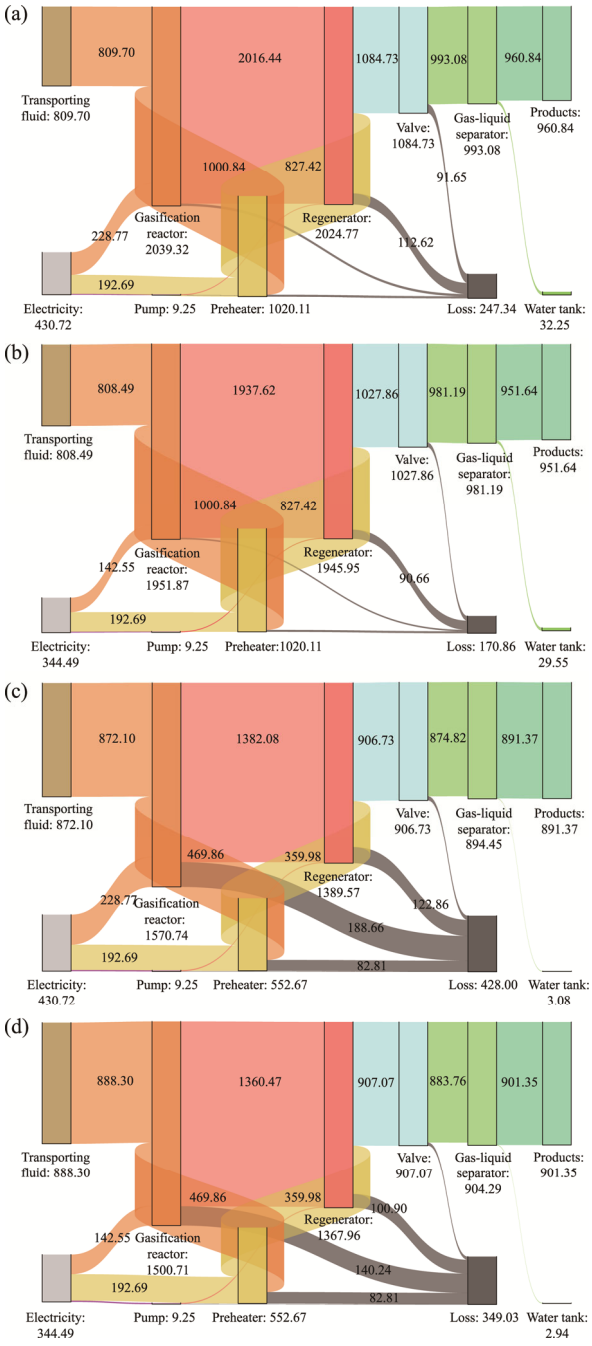


**Fig. 9** Energy flow of the system transported by (a) $H_2O$; (b) $CO_2$, and Exergy flow of the system transported by (c) $H_2O$; (d) $CO_2$ (Unit: kW)

point. Both the hot flow and cold flow contained much $H_2O$, much heat would cost during trans-criticality. Temperature of the two flows might reach the critical temperature in the regenerator and heat could not be transferred if the temperature difference was reduced. It was necessary to determine the heat transfer temperature difference and reduce the energy loss from regenerator. The output of the hot flow in regenerator was mainly pressured $H_2O$ and the pressure of this flow was reduced

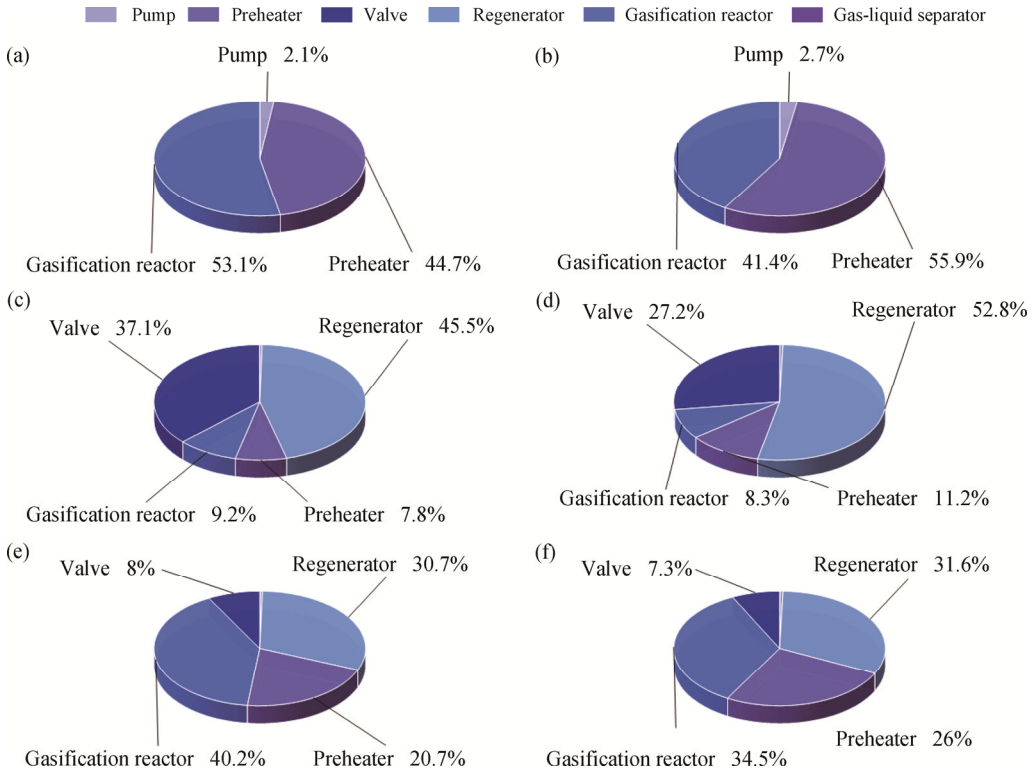


**Fig. 10** Distribution of electricity consumption of the system with (a) $H_2O$ transporting (b) $CO_2$ transporting; Distribution of energy loss of the system with (c) $H_2O$ transporting (d) $CO_2$ transporting; Distribution of exergy loss of the system with (e) $H_2O$ transporting (f) $CO_2$ transporting

in the valve. This part of energy could be recovered if the valve was replaced into hydraulic turbine. The increase of the efficiency of preheater and gasification reactor also decreased the energy loss of the models. Ways to reduce the exergy loss of these models were the same with those of reducing the energy loss.

## 5. Conclusion

A supercritical water gasification system, in which $CO_2$ was used as the transporting medium, was investigated from the point of view of thermodynamics in this paper. In this way, heat input by a large specific heat capacity and trans-criticality of transporting $H_2O$ could be saved. In this work, influence on gasification results was investigated and the influencing factors were selected as reaction temperature, pressure, transporting and gasification concentration. Furthermore, a similar system with $H_2O$ transporting was also based to compare and study the difference between the two systems. The results were as follows:

(1) Total yield, HE and the electricity consumption of gasification reactor increased with temperature sharply and decreased with pressure slightly. Total yield increased from 174.05 kg/h at 823.15 K and 23 MPa to 224.32 kg/h at 1073.15 K and 23 MPa. The total yield decreased from 191.79 kg/h at 923.15 K and 23 MPa to 187.31 kg/h at 923.15 K and 29 MPa. Increase of the transporting concentration led to the increase of the total yield and HE and the decrease of electricity consumption. Yields of each production increased with gasification concentration, so did the electricity consumption. But HE decreased at the same time. Total yield increased from 184.42 kg/h to 192.32 kg/h when the ratio between the sample and transporting medium increased from 20 wt% to 120 wt%. And it increased from 75.84 kg/h to 236.69 kg/h with the increase of gasification concentration from 30 wt% to 120 wt%.

(2) The production yields and the heat absorption of gasification reaction were influenced slightly in both systems whose transporting medium was $CO_2$ and $H_2O$, respectively. The energy efficiency of double systems was 77.4% in $H_2O$-transporting system and 82.53% in $CO_2$-transporting system, respectively. The exergy efficiency was 68.42% and 73.11%, respectively. $CO_2$-transporting system could indeed save the energy and maintain the output of the products.

(3) Electricity consumption concentrated on gasification reactor and preheater while energy loss was mainly distributed to regenerator, valve, gasification reactor and preheater. Exergy loss of the system was mainly made up with the loss of gasification reactor,

regenerator, preheater and valve. Three ways to decrease the electricity consumption, heat loss and exergy loss were investigated, which were the increase of the efficiency of the models, the reduction of the temperature difference of regenerator and changing the valve into hydraulic turbine.

## Acknowledgment

This work is supported by the Basic Science Center Program for Ordered Energy Conversion of the National Natural Science Foundation of China (No. 51888103).

## Conflict of Interest

On behalf of all authors, the corresponding author states that there is no conflict of interest.

## References

[1] Luderer G., Madeddu S., Merfort L., Ueckerdt F., Pehl M., Pietzcker R., Rottoli M., Schreyer F., Bauer N., Baumstark L., Bertram C., Dirnaichner A., Humpenöder F., Levesque A., Popp A., Rodrigues R., Strefler J., Kriegler E., Impact of declining renewable energy costs on electrification in low-emission scenarios. Nature Energy, 2022, 7: 32–42.

[2] Zhou H., Dong P., Zhu S., Li S., Zhao S., Wang Y., Design and theoretical analysis of a liquid piston hydrogen compressor. Journal of Energy Storage, 2021, 41: 102861.

[3] Aydin M.I., Karaca A.E., Qureshy A.M.M.I., Dincer I., A comparative review on clean hydrogen production from wastewaters. Journal of Environmental Management, 2021, 279: 111793.

[4] Cao W., Wang S., Ma L., Liu S., Jin H., Wei W., Guo L., Catalytic gasification of phenol in supercritical water with different metal cations. Fuel, 2022, 324: 124754.

[5] Cao W., Wei Y., Jin H., Liu S., Li L., wei W., Guo L., Characteristic of food waste gasification in supercritical water for hydrogen production. Biomass and Bioenergy, 2022, 163: 106508.

[6] Lu B., Ge Z., Chen Y., Shi J., Jin H., Study on supercritical water gasification reaction and kinetic of coal model compounds. Fuel Processing Technology, 2022, 230: 107210.

[7] Wang W., Bai B., Wei W., Cao C., Jin H., Hydrogen-rich syngas production by gasification of Urea-formaldehyde plastics in supercritical water. International Journal of Hydrogen Energy, 2021, 46: 35121–35129.

[8] Toor S.S., Rosendahl L., Rudolf A., Hydrothermal liquefaction of biomass: A review of subcritical water technologies. Energy, 2011, 36: 2328–2342.

[9] Xu C., Donald J., Upgrading peat to gas and liquid fuels in supercritical water with catalysts. Fuel, 2012, 102: 16–25.

[10] Dorotić H., Pukšec T., Duić N., Economical, environmental and exergetic multi-objective optimization of district heating systems on hourly level for a whole year. Applied Energy, 2019, 251: 113394.

[11] Guo L., Jin H., Boiling coal in water: Hydrogen production and power generation system with zero net $CO_2$ emission based on coal and supercritical water gasification. International Journal of Hydrogen Energy, 2013, 38: 12953–12967.

[12] Aziz M., Integrated supercritical water gasification and a combined cycle for microalgal utilization. Energy Conversion and Management, 2015, 91: 140–148.

[13] Rahbari A., Venkataraman M.B., Pye J., Energy and exergy analysis of concentrated solar supercritical water gasification of algal biomass. Applied Energy, 2018, 228: 1669–1682.

[14] Peng Z., Xu J., Rong S., Luo K., Lu L., Jin H., Zhao Q., Guo L., Thermodynamic and environmental analysis for multi-component supercritical thermal fluid generation by supercritical water gasification of oilfield wastewater. Energy, 2023, 269: 126766.

[15] Moghaddam E.M., Goel A., Siedlecki M., Michalska K., Yakaboylu O., de Jong W., Supercritical water gasification of wet biomass residues from farming and food production practices: lab-scale experiments and comparison of different modelling approaches. Sustainable Energy & Fuels, 2021, 5: 1521–1537.

[16] Liang J., Liu Y., Chen J., E J., Leng E., Zhang F., Liao G., Performance comparison of black liquor gasification and oxidation in supercritical water from thermodynamic, environmental, and techno-economic perspectives. Fuel, 2023, 334: 126787.

[17] Jiang K., Shi J., Zhao Q., Jin H., Research progress of industrial application based on two-phase flow system of supercritical carbon dioxide and particles. Powder Technology, 2022, 407: 117621.

[18] Song X.Z., Li G.S., Guo B., Wang H.Z., Li X.J., Lü Z.H., Transport feasibility of proppant by supercritical carbon dioxide fracturing in reservoir fractures. Journal of Hydrodynamics, 2018, 30: 507–513.

[19] Shen Z., Wang H., Li G., Numerical simulation of the cutting-carrying ability of supercritical carbon dioxide drilling at horizontal section. Petroleum Exploration and Development, 2011, 38: 233–236.

[20] Wang H., Wang M., Yang B., Lu Q., Zheng Y., Zhao H., Numerical study of supercritical $CO_2$ and proppant transport in different geometrical fractures. Greenhouse Gases: Science and Technology, 2018, 8: 898–910.

[21] Shieh P., Zhang W., Husted K.E.L., Kristufek S.L., Xiong B., Lundberg D.J., Lem J., Veysset D., Sun Y., Nelson K.A., Plata D.L., Johnson J.A., Cleavable comonomers enable degradable, recyclable thermoset plastics. Nature, 2020, 583: 542–547.

[22] Pérez R.L., Ayala C.E., Opiri M.M., Ezzir A., Li G., Warner I.M., Recycling thermoset epoxy resin using alkyl-methyl-imidazolium ionic liquids as green solvents. ACS Applied Polymer Materials, 2021, 3: 5588–5595.

[23] Tang K., Zhang A., Ge T., Liu X., Tang X., Li Y., Research progress on modification of phenolic resin. Materials Today Communications, 2021, 26: 101879.

[24] Xu Y., Guo L., Zhang H., Zhai H., Ren H., Research status, industrial application demand and prospects of phenolic resin. RSC Advances, 2019, 9: 28924–28935.

[25] Ozaki J.-i., Djaja S.K.I., Oya A., Chemical recycling of phenol resin by supercritical methanol. Industrial & Engineering Chemistry Research, 2000, 39: 245–249.

[26] Zhang J., Li X., Song D., Miao Y., Song J., Zhang L., Effective regeneration of anode material recycled from scrapped Li-ion batteries. Journal of Power Sources, 2018, 390: 38–44.

[27] Liu X., Li Y., Xing X., Zhang G., Jing X., Fully recyclable and high performance phenolic resin based on dynamic urethane bonds and its application in self-repairable composites. Polymer, 2021, 229: 124022.

[28] Chen J., Zhang K., Zhang K., Jiang B., Huang Y., Facile preparation of reprocessable and degradable phenolic resin based on dynamic acetal motifs. Polymer Degradation and Stability, 2022, 196: 109818.

[29] Wang W., Wang C., Huang Y., Lu H., Chen J., Shi J., Jin H., Heat, electricity, and fuel gas ploy-generation system on an island based on plastic waste gasification in supercritical water. ACS Sustainable Chemistry & Engineering, 2022, 10: 13786–13791.

[30] Chen J., Liu Y., Wu X., E J., Leng E., Zhang F., Liao G., Thermodynamic, environmental analysis and comprehensive evaluation of supercritical water gasification of biomass fermentation residue. Journal of Cleaner Production, 2022, 361: 132126.

[31] Kruse A., Meier D., Rimbrecht P., Schacht M., Gasification of pyrocatechol in supercritical water in the presence of potassium hydroxide. Industrial & Engineering Chemistry Research, 2000, 39: 4842–4848.

[32] Xu J., Peng Z., Rong S., Jin H., Guo L., Zhang X., Zhou T., Model-based thermodynamic analysis of supercritical water gasification of oil-containing wastewater. Fuel, 2021, 306: 121767.